Biochimica et Biophysica Acta 1798 (2010) 122–127

Contents lists available at ScienceDirect

Biochimica et Biophysica Acta

journal homepage: www.elsevier.com/locate/bbamem

NMR structure of the transmembrane and cytoplasmic domains of human CD4 in micelles

Marc Wittlich [a,b], Pallavi Thiagarajan [a,b], Bernd W. Koenig [a,b], Rudolf Hartmann [a], Dieter Willbold [a,b,*]

[a] Forschungszentrum Jülich, Institut für Strukturbiochemie (ISB-3), 52425 Jülich, Germany
[b] Heinrich-Heine-Universität Düsseldorf, Institut für Physikalische Biologie, BMFZ, 40225 Düsseldorf, Germany

ARTICLE INFO

Article history:
Received 9 July 2009
Received in revised form 31 August 2009
Accepted 15 September 2009
Available online 23 September 2009

Keywords:
CD4
HIV-1
VpU
Membrane protein
NMR

ABSTRACT

The human cluster determinant 4 (CD4) is a type I transmembrane glycoprotein involved in T-cell signalling. It is expressed primarily on the surface of T helper cells but also on subsets of memory and regulatory T lymphocytes ($CD4^+$ cells). It serves as a coreceptor in T-cell receptor recognition of MHC II antigen complexes. Besides its cellular functions, CD4 serves as the main receptor for human immunodeficiency virus type I (HIV-1). During T-cell infection, the CD4 extracellular domain is bound by HIV-1 gp120, the viral surface glycoprotein, which triggers a number of conformational changes ultimately resulting in virion entry of the cell. Subsequently, CD4 is downregulated in infected cells by multiple strategies that involve direct interactions of the HIV-1 proteins VpU and Nef with the cytoplasmic part of CD4. In the present work, we describe the NOE-based solution structure of the transmembrane and cytoplasmic domains of the cystein-free variant of CD4 (CD4mut) in dodecylphosphocholine (DPC) micelles. Furthermore, we have characterized micelle-inserted CD4mut by paramagentic relaxation enhancement (PRE) agents and ^1H-^{15}N heteronuclear NOE data. CD4mut features a stable and well-defined transmembrane helix from M372 to V395 buried in the micellar core and a cytoplasmic helix ranging from A404 to L413. Experimental data suggest the amphipathic cytoplasmic helix to be in close contact with the micellar surface. The role of the amphipathic helix and its interaction with the micellar surface is discussed with respect to the biological function of the full-length CD4 protein.

1. Introduction

Still, membrane proteins represent very challenging objects for high-resolution structure determinations. In the current study, we use liquid-state nuclear magnetic resonance (NMR) spectroscopy to investigate the 3D structure of a micelle-inserted transmembrane protein combined with dynamical data. High-resolution NMR approaches provide diverse data on integral membrane proteins (IMPs). The chemical shift values are sensitive to backbone torsion angles [1] and can be used for identification of secondary structure elements. NOESY spectra contain information on proton–proton distances and yield input for restrained molecular dynamics-based structure calculation [2]. Confinement of micelle- or bicelle-incorporated IMP in an asymmetric environment, e.g., a stressed polyacrylamide gel [3,4], allows measurement of residual dipolar couplings, which are sensitive to bond vector orientation to assist the determination of the 3D structure of the protein backbone [5]. The location and topology of the helices are derived from periodic patterns in the dipolar couplings [6]. High-resolution NMR measurements of relaxation times and ^1H-^{15}N heteronuclear NOEs give detailed insight into local backbone dynamics [7,8]. Protein–protein interactions can be addressed by liquid-state NMR. A variety of approaches has been used for detection of binding, for mapping of the binding site onto the surface of the interaction partners, and even in-depth characterization of the complex structure [9,10].

Reconstitution of membrane proteins in a suitable environment has always been a field of very broad interest. Not only for structural studies, IMPs have to be properly folded upon reinsertion to maintain biological functionality. This requires the choice of suitable lipids or lipid mixtures for IMP embedding. In addition, the overall mass of the IMP-bearing particle must be small enough to ensure short rotational correlation times, if liquid-state NMR methods ought to be used. Then even small liposomes are too large in molecular weight. Instead, numerous membrane-mimicking conditions have been explored to allow solubilization of the IMP while closely matching the physico-chemical environment of the membrane and, at the same time, being suitable for liquid-state NMR. Reviews on the available options for membrane protein solubilization [11–13] and evaluations of a multitude of detergents for solution NMR studies on IMPs [14, 15] have been published. Detergent micelles have been used to study

Abbreviations: CD4, cluster determinant 4; DPC, dodecylphosphocholine; ER, endoplasmatic reticulum; IMP, integral membrane protein; LB, Luria-Bertani; Lck, lymphocyte specific kinase; MHC II, class II major histocompatibility complex; PFG, pulsed field gradient; RPC, reversed phase chromatography; 2D, two-dimensional; 3D, three-dimensional; TFE, 2,2,2-trifluoroethanol; VpU, viral protein U

* Corresponding author. Forschungszentrum Jülich, Institut für Strukturbiochemie (ISB-3), 52425 Jülich, Germany. Tel.: +49 2461 612100; fax: +49 2461 612023.
E-mail address: dieter.willbold@uni-duesseldorf.de (D. Willbold).

0005-2736/$ – see front matter © 2009 Elsevier B.V. All rights reserved.
doi:10.1016/j.bbamem.2009.09.010

IMPs with only one [16], sometimes two [2] or even more membrane spanning helices [17], as well as β-barrel proteins [18].

In the present study, we gathered detailed structural and dynamic information of the human cluster determinant 4 (CD4) protein. CD4 is a 433-residue type I transmembrane glycoprotein involved in T-cell signalling of MHC-II-restricted T lymphocytes [19]. The function of these $CD4^+$ T-cells relies on the direct interaction between CD4 and the major histocompatibility complex type II (MHC-II) presenting an antigen on the surface of a macrophage [20]. The extracelluar segment of CD4, consisting of 371 amino acid residues, contains four immunoglobulin-like domains [21]. This ectodomain participates in a complex with the antigen-specific T-cell receptor (TCR) and serves as coreceptor that binds to the non-polymorphic region of MHC-II.

In addition to its cellular functions, CD4 is the major receptor for human immunodeficiency virus type I (HIV-1) [22,23]. Thus, CD4 is targeted by several HIV-1-coded proteins. HIV-1 negative factor (Nef) binds directly to the cytoplasmic part of CD4 and downregulates CD4 from the cell surface [24,25]. HIV-1 viral protein U (VpU) also binds directly to CD4 cytoplasmic domain to prevent further delivery of newly synthesized CD4 from the ER to the cell surface by inducing CD4 degradation via the ubiquitin-dependent proteasomal pathway [26,27]. The CD4 sequence region responsible for this function is located between amino acid residues 402 to 420 [28]. From mutational analysis, it is known that residues 407 to 418 in the cytoplasmic domain of CD4 are necessary and sufficient for down-regulation of CD4 by Nef [24,25,29]. The di-leucine motif at sequence positions 413 and 414 of CD4 plays a crucial role in Nef binding [30].

Previously, we employed secondary chemical shift analysis for identification of secondary structure elements within residues 372 to 433 of CD4mut, which resembles the transmembrane and cytoplasmic domains of CD4 with its five cysteines being conservatively replaced by four serines and one histidine [31]. Two helices were found ranging from amino acid residue 372 to 395 and from residue 407 to 412, reflecting the transmembrane and cytoplasmic helices of CD4, respectively [32]. The aim of the current study is characterization of the 3D structure of CD4mut based on proton–proton distance constraints from nuclear Overhauser enhancement (NOE) data. In addition, information on CD4mut has been collected based on heteronuclear ^{1}H-^{15}N-NOE data, water protection factors, and enhancement of spin relaxation by paramagnetic probes.

2. Materials and methods

Perdeuterated dodecylphosphocholine (DPC-d38), ^2H_2O, [U-^{13}C] glucose and [U-^{15}N] ammonium chloride were purchased from Cambridge Isotope Laboratories. HPLC grade organic solvents were used. All other chemicals were graded analytical or better.

2.1. Expression and purification of CD4mut

CD4mut covers residues 372 to 433 of human CD4 comprising the transmembrane and cytoplasmic domains with five cysteines being conservatively replaced by four serines and one histidine [31]. CD4mut was expressed in *Escherichia coli* as a fusion protein containing an N-terminal His-tag, ubiquitin, and a short linker containing protease cleavage sites. After enzymatic cleavage of the fusion protein with PreScission protease, the eight amino acid residues GPLVPRGS remain at the aminoterminal end of CD4mut: MALIVLGGVAGLLLFIGLGIFFSVRSRHRRRQAERMSQIKRLL-SEKKTSQSPHRFQKTHSPI with all residues given in the one-letter code.

The purification of CD4mut comprises detergent-based cell lysis, metal affinity purification of the fusion protein, a desalting step, PreScission cleavage, TCA precipitation, and reversed phase chromatography. About 8 mg of uniformly ^{13}C, ^{15} N-labeled CD4mut was regularly obtained per liter of isotope-labeled M9 minimal medium. Details on cloning, expression, and purification of CD4mut have been published [31,32].

2.2. NMR sample preparation

The NMR sample contained 1 mM of CD4mut in 90% H_2O/10 % ^2H_2O micellar solution (200 mM DPC-d38, 20 mM sodium phosphate, 150 mM NaCl, 0.02% (w/v) NaN_3, pH 6.2). The sample was transferred to a (3×6) mm^2 ^2H_2O-matched Shigemi S-tube (Varian Inc., Palo Alto, USA) or 5 mm Shigemi tube after adjusting the pH to 6.2. Some experiments were conducted in ^2H_2O after lyophilizing and redissolving the sample in 99.996% ^2H_2O. Additional experiments were carried out with CD4mut in SDS micelles (200 mM SDS, 20 mM sodium phosphate, 150 mM NaCl, 0.02% (w/v) NaN_3, pH 6.5).

2.3. Data acquisition and processing

NMR spectra for sequential resonance assignment were acquired at 14.1 T, while NOESY spectra for obtaining distance constraints were acquired at 14.1 T and 18.8 T. Experiments were conducted at 45 °C on Varian Unity INOVA spectrometers using cryogenically cooled 5 mm Z-PFG-^{1}H{^{13}C, ^{15}N} probes.

The resonance assignment strategy has been described earlier [32]. Shortly, a set of standard 2D and 3D spectra based on a transverse relaxation-optimized (TROSY) [33] variant of the ^{1}H, ^{15}N-HSQC [34] was recorded for backbone assignment, while 2D and 3D ^{1}H, ^{13}C-HSQC-based [35] spectra were acquired for the side chain assignment. Proton–proton distances were extracted from gradient-enhanced 3D ^{15}N-NOESY-HSQC spectra [36] acquired with a mixing time of 150 ms, and from 3D gradient-enhanced ^{13}C-resolved HSQC-NOESY spectra [37] recorded with a mixing time of 120 ms. Data were processed with NMRPipe [38] and VNMRJ (Varian Inc.) and CARA was used for spectral analysis and resonance assignment [39].

2.4. NOE assignment and structure calculation

Interproton distances were derived from NOESY data using RADAR, an automated NOESY spectral analysis software. RADAR combines ATNOS [40] for automated NOESY peak picking and NOE signal identification in NOESY spectra, CANDID [41] for combined automated NOE assignment and structure calculation, and the torsion angle dynamics-based simulation algorithm CYANA [42]. RADAR runs an iterative process consisting of seven cycles. Within a cycle, ATNOS performs a baseline correction and signal-to-noise estimation, as well as identification of potential NOE signals in concordance with the user-provided chemical shift assignment table. CANDID uses the chemical shift table and the presence of symmetrical cross-correlations, as well as the compatibility with the polypeptide chain for assignment of NOE correlations. The subsequent integration and calibration of the signals result in a list of upper distance constraints [42] without artefacts and ambiguous constraints. The set of upper distance constraints serves as input for torsion angle dynamics with CYANA. The resulting structure ensemble is utilized for identification and assignment of NOE resonances in the next cycle of RADAR.

After the last automatic iteration step, the set of upper distance constraints was further examined manually in an interactive and iterative process. CYANA was used to calculate 100 structures based on the NOE data. The ensemble of the 20 least energy conformers was deposited in the Protein Data Bank (PDB) under accession code 2klu. MOLMOL [43] was used for visualization and analysis of the structural ensemble.

2.5. Determination of hetero-NOEs

Heteronuclear ^{1}H-^{15}N NOEs were derived from 2D spectra acquired at 18.8 T using a TROSY-based [33] NOE pulse sequence

[44]. The spectra were recorded with or without 3 s of proton saturation with a series of 120° pulses spaced at 5-ms intervals prior to the first pulse of the NOE sequence, respectively. NOE intensities were obtained by fitting these peaks to an adjustable "model peak" shape in CARA [39]. A superposition of Gauss and Lorentz functions was employed, where Gauss-Lorentz balance and line width can easily be adjusted manually and independently for both spectral dimensions. Finally, a complete list of ^{1}H-^{15}N-NOE intensities was obtained for both spectra, and the heteronuclear NOE was derived as the ratio of the integral peak intensities measured with and without proton saturation, respectively:

$$NOE = \frac{I_{sat}}{I_{unsat}}$$

Standard deviation values for NOE were determined as follows:

$$\frac{\Delta NOE}{NOE} = \sqrt{\left(\frac{\sigma_{Isat}}{I_{sat}}\right)^2 + \left(\frac{\sigma_{Iunsat}}{I_{unsat}}\right)^2}$$

2.6. Determination of water protection factors

Labile amide protons easily exchange with protons of the water. Engagement of these protons in hydrogen bonds of regular secondary structure elements such as alpha helices or beta sheets results in protection from exchange and thus in a longer "lifetime" of the respective amide proton signals.

Amide cross peak intensities were derived from ^{1}H, ^{15}N-TROSY-HSQC spectra. First, an HSQC spectrum of CD4mut in DPC micelles was recorded in buffer containing 90% H_2O/10% $^{2}H_2O$. Subsequently, the sample was lyophilized and redissolved in 100% $^{2}H_2O$. HSQC spectra were recorded immediately after reinsertion of the sample into the magnet, and after 1, 2, and 4 h.

2.7. DPC micelle interaction of CD4mut

The position of CD4mut with respect to the micelle was studied using the paramagnetic relaxation agents 16- and 5-doxylstearic acid, respectively. Paramagnetic relaxation enhancement (PRE) causes broadening of protein NMR signals in the vicinity of the probe. The PRE is quantified in terms of signal retention in HSQC spectra recorded with and without the paramagnetic agent in the sample, respectively [45]. In initial experiments, we tested a range of concentration between 0.2 and 8 mM for both agents. The final data were recorded with a molecular ratio between paramagnetic relaxation agents and protein of 5:1.

3. Results and discussion

3.1. Secondary structure of CD4mut determined by NOE-derived constraints

Nearly complete resonance assignment of DPC micelle-inserted CD4mut has been reported earlier [32]. Secondary chemical shift analysis predicted a transmembrane α-helix from 372 to 395 and a short α-helix from residue 407 to 412.

To verify the existence of the predicted secondary structure elements and to obtain potential tertiary structural data, NOE data have been collected of CD4mut in DPC micelles in the present study. For the structure calculations, a total of 623 NOE distance constraints have been used. Another 233 dihedral constraints were derived from chemical shift data using the program TALOS [46], which is implemented in the RADAR routine, and included in the calculation of the final structure. A final ensemble of 20 NMR structures with the lowest CYANA target functions were used to characterize the structure of CD4mut in DPC micelles. None of the 20 structures violated NOE distances by more than 0.030 nm. No dihedral-angle constraint was violated more than 5°. A summary of the experimental constraints and structural statistics is given in Table 1. Long-range NOE contacts could not be observed. Therefore, the overall structure ensemble does not converge to a unique conformer. However, well-defined secondary structure elements were obtained from the structure calculations.

The transmembrane helix comprising residues M372 to V395 is reasonably well defined with an average root-mean-squared deviation (RMSD) of 0.3 nm for the backbone atoms (Fig. 1). Notably, the side chain of F392 strongly points towards the C-terminus of the helix, while usually side chains of residues involved in helical structures point towards the amino-terminus (Fig. 1). The alignment between the voluminous side chains of F392, F393 and R396 is well defined by direct NOE correlations. In particular, the NOE correlations giving rise to this structural feature are F392-CH^{α} — V395-CH^{β}, F392-CH^{α} — V395-CH_3^{γ}, F392-CH_2^{δ} — R396-CH_2^{δ}, F392-CH_2^{ε} — R396-CH_2^{δ}, F393-CH^{α} — R396-CH_2^{β}, F393-CH^{α} — R396-CH_2^{γ}, and F393-CH_2^{δ} — R396-CH_2^{δ}.

The tilt of the long axis of a transmembrane helix with respect to the membrane normal might play an important role for membrane protein function and molecular interactions. Unfortunately, solution NMR on integral membrane proteins in a micellar environment cannot answer this question. In the future, however, we plan to complement our results with solid-state NMR data obtained on CD4 in liposomes. Combination of experimental restraints from solution and solid-state NMR data with molecular dynamics simulation might very well allow a more detailed understanding of CD4 structure and interactions [47].

A second helix ranging from residue A404 to L413 is defined with an RMSD value of 0.6 nm in the cytoplasmic part of the molecule (Fig. 2). Although in the finally obtained structure ensemble the typical α-helical hydrogen bonding pattern is present only for residues M407 to R412, helical conformation together with a decreased RMSD value is observed for residues A404 to L413 (Fig. 2). Because of the absence of long-range NOEs between residues of this helix and those of the transmembrane helix, the relative orientation between both helices is not defined.

The structure of the cytoplasmic domain has been subject to earlier investigations by NMR and CD spectroscopy using the soluble synthetic peptides CD4(403–419) [48] and CD4(396–433) [49,50]. Willbold and Rösch identified an α-helix in aqueous solution ranging from Q403 to R412. Wray et al. studied the cytoplasmic domain of CD4 in water and trifluoroethanol (TFE) solution. In aqueous solution, the peptide was reported to be unstructured [49,50], while helical conformation was adopted in presence of buffer containing TFE. In presence of 50 vol.% TFE, an α-helix is induced containing residues R402 to K417 [50]. In sum, the cytoplasmic helix derived in the present study is in reasonable agreement with previous studies.

Table 1
Summary of structural statistics of CD4mut in DPC micelles.

Experimental restraints	
Total NOE restraints	623
Intraresidue	231
Sequential	214
Medium range ($2 \le \lvert i-j \rvert \le 5$)	178
CYANA structural statistics	
Target function	0.017 ± 0.008 nm^2
Sum of NOE violations >0.015 nm	0.13 nm
Maximum violation	0.03 nm
RMSD to mean structure (nm) (backbone only/ all heavy atoms)	
M372-V395	0.355/0.608
R396-Q403	2.028/4.108
A404-L413	0.622/1.356
L414-I433	3.950/5.066

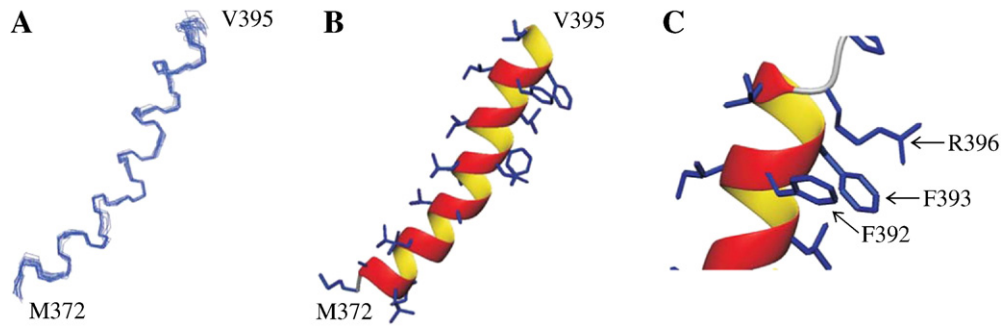

Fig. 1. Structure of the transmembrane helix of CD4mut calculated from NOE-derived upper distance constraints. (A) Ensemble of the 20 lowest energy conformers from torsion angle dynamics. Superposition is based on minimization of the RMSD between all backbone heavy atoms of M372 to V395 with respect to the lowest energy conformer. (B) Ribbon representation of one representative conformer of the transmembrane helix of CD4mut. Bonds between heavy atoms in the side chains are shown by sticks. (C) C-terminal end of the transmembrane helix. Side chains of F392, F393, and R396 are marked.

In addition, we used heteronuclear ^{1}H-^{15}N-NOEs as a measure for local backbone dynamics on the pico- to nanosecond time scale [7]. Positive ^{1}H-^{15}N NOEs close to the value of 0.8 indicate the respective residue to be contained in a rigid structure. Thus, a rigid structure can be inferred for most of the transmembrane residues. The residues forming the cytoplasmic helix and the interhelical region show heteronuclear NOE values around 0.5, which indicates only a small degree of flexibility, even at 45 °C. Rapid internal motion will reduce the heteronuclear NOE, which may even become negative for highly mobile residues exhibiting large amplitude motions on the sub-nanosecond time scale [51]. Such a behaviour is observed towards the C-terminal end of the CD4mut protein. The respective heteronuclear NOE values demonstrate this region to be highly flexible (Fig. 3).

3.2. Structure of the inter-helix region

The structure of CD4mut is dominated by two helical segments M372 to V395 and A404 to L413. The NOE pattern of the interhelical region does not indicate any regular secondary structure elements. The average hetero-NOE in this region is reduced and amounts to ~0.3. Apparently, the interhelical linker exhibits some structural flexibility but it is not completely mobile. The short interhelical region R396-SRHRRR-Q403 is located at the polar lipid–water interface. Thus, it is in contact with the zwitterionic DPC head groups and water molecules. The interhelical region contains a dense cluster of positive charges. This high net charge might prevent secondary structure formation. The situation might be quite different at the negatively charged surface of the ER membrane. Therefore, we also studied CD4mut inserted in negatively charged sodium dodecyl sulfate (SDS) micelles. In particular, we analyzed secondary chemical shifts of CD4mut residues located in the two helices and the interhelical linker.

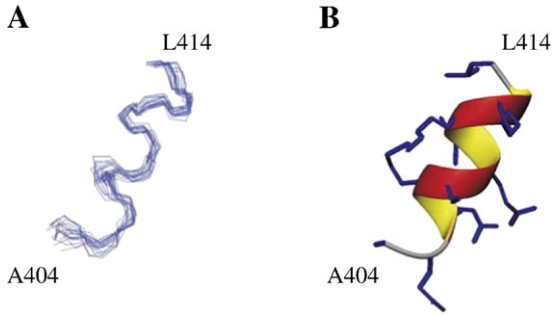

Fig. 2. Structure of the cytoplasmic helix from torsion angle dynamics. (A) Twenty lowest energy conformers are shown. Superposition is based on all backbone heavy atoms of A404 to L414. (B) Ribbon representation of one representative conformer. Side chain bonds are shown as sticks. The conformer is in the same orientation as the bundle in panel (A).

The pattern of secondary chemical shifts of CD4mut in SDS is very similar to the pattern observed in DPC (data not shown). The only notable difference is an extension of the transmembrane helix by two residues (396 and 397). However, no indications for helical structure of the remaining residues 398 to 403 of the linker were found neither in DPC nor SDS. We conclude that the interhelical region remains non-helical independent of the presence of negatively charged lipids.

3.3. CD4mut interaction with the micelle

To probe the interaction of CD4mut with DPC micelles, we used 16- and 5-doxyl stearic acid to map residues that are deeply buried

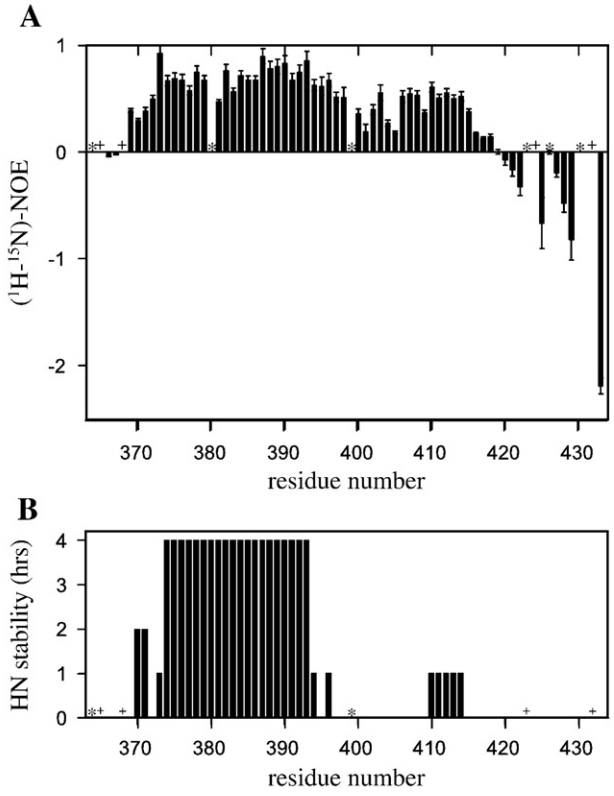

Fig. 3. ^{1}H -^{15}N-hetero-NOE values and amide proton exchange times of CD4mut in DPC micelles. (A) ^{1}H-^{15}N-hetero-NOE values of backbone amides of CD4mut in DPC micelles. Intensities of residues marked with an asterisk (*) could not be derived due to heavy spectral overlap. Proline residue positions are marked with a plus (+). (B) Exchange times of amide protons of CD4mut in DPC micelles. Intensities of residues marked with an asterisk (*) could not be derived due to heavy spectral overlap. Proline residue positions are marked with a plus (+).

in the micelle or closer to the micelle surface, respectively [45]. It can be expected that 16-doxyl stearic acid causes a reduction in the resonance intensities of amino acids located nearby the micellar core. 5-Doxyl stearic acid, however, will also cause resonance intensity reduction of residues near the micellar core, but residues closer to the micelle surface are expected to be even more affected. Fig. 4 summarizes the results. Residues 380 to 390 are most affected by 16-doxyl stearic acid, while intensity retention becomes smaller towards the ends of the micelle spanning helix (Fig. 4A). Unexpectedly, residues from R369 towards the N-terminus of the protein experienced intensity retention. Possibly, because of the elongated chain length of 16-doxyl stearic acid in comparison to the hydrophobic part of DPC, a fraction of 16-doxyl stearic acid molecules are oriented unexpectedly. This may also explain why virtually all residues of CD4mut, except the very C-terminal residues, are affected by an overall reduction of their signal intensities. The pattern of residues affected by 5-doxyl stearic acid is exactly as expected. Residues 380 to 390 in the center of the micelle are hardly affected, but residues around 370 and 399, which are expected to be close to the micelle water interface, are significantly affected. Remarkably, there is an interesting periodicity of the resonance intensity reductions for residues of the cytoplasmic helix A404 to L413 (404, 407, 409, 410, 413), which is in agreement with close proximity of this α-helix to the micellar surface (Fig. 4B). The C-terminal region of the protein is virtually unaffected by the paramagnetic agents. The signal intensity reductions induced by 16-doxyl stearic acid have been mapped onto the surface of a low-energy CD4mut conformation (Fig. 5A). For comparison, the surface electrostatic potential map of CD4mut is illustrated in Fig. 5B.

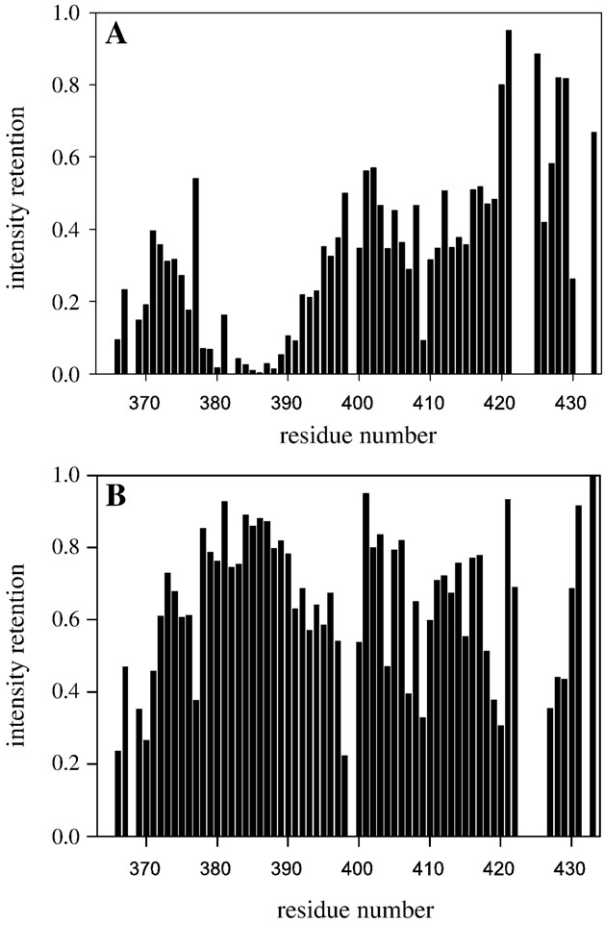

Fig. 4. Paramagnetic relaxation enhancement obtained for CD4mut in DPC micelles using 16- and 5-doxylstearic acid. Intensity retention is plotted as a function of amino acid sequence position. (A) Intensity retention plot for CD4mut in the presence of 5 mM 16-doxylstearic acid (5:1 relaxation agent/protein molar ratio). (B) Intensity retention plot for CD4mut in the presence of 5 mM 5-doxylstearic acid (5:1 relaxation agent/protein molar ratio).

3.4. H/D exchange experiments

The stability of hydrogen bonds of CD4mut in DPC micelles was assayed by H/D exchange experiments. Labile hydrogens rapidly exchange with solvent atoms. After transferring a protein from H_2O to ^2H_2O, such protons rapidly exchange for deuterons, that is, they become invisible in ^1H, ^{15}N-HSQC spectra. Protons involved in stable hydrogen bonds are partially protected from exchange and may be detected in the spectra for a prolonged period after solvent exchange. HSQC signal intensity was measured as a function of time after solvent exchange and is presented as a function of residue number in Fig. 3B. The plot clearly shows two regions with reduced hydrogen exchange rates. Backbone amide protons of the transmembrane helix are observable for several hours after solvent exchange. Residues in the center of the amphipathic helix withstand exchange for about an hour. These observations are in agreement with the proposed burial of the transmembrane helix in the hydrophobic interior of the micelle and a location of the cytoplasmic helix at the micelle water interface [52].

In summary, the structure of the transmembrane and cytoplasmic domains of CD4 can be described by a very stable and rigid transmembrane α-helix (372–395) and a second cytoplasmic α-helix (403–413), which is reasonably stable even at 45 °C supported by helix-type NOE patterns, H/D exchange experiments, and heteronuclear NOE values. Obviously, the amphipathic character of the helix tethers the structure to the micellar surface. Notably, the region in HIV-1 VpU, which is responsible for CD4 binding, also features a long amphipathic helix [53,54]. Confining the two amphipathic helices to the polar membrane interface might be crucial for productive

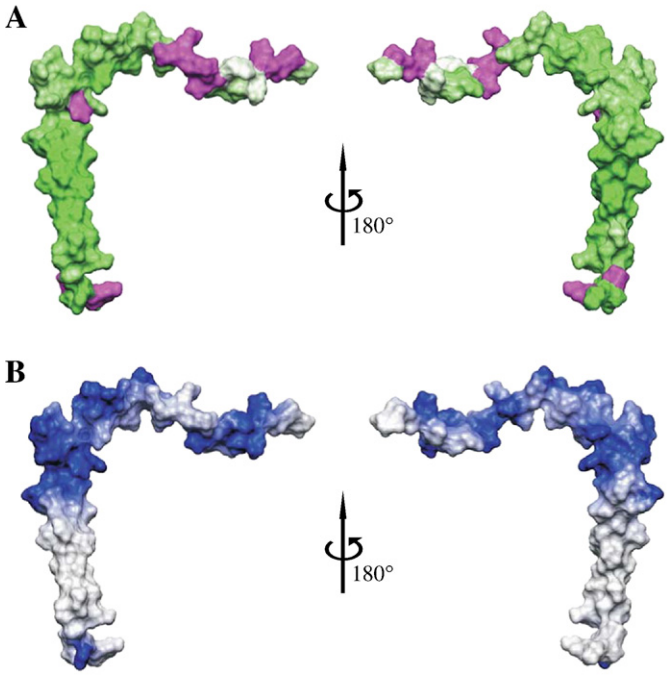

Fig. 5. Surface representation of paramagnetic quenching and electrostatic potential for CD4mut residues. (A) The degree of NMR signal quenching is indicated by different shades of green colour. Dark green indicates maximum quenching, while light green symbolizes intermediate effects. White is used to indicate absence of quenching. Amino acid residues that could not be evaluated are coloured in magenta. (B) Electrostatic potential plot of CD4mut shows a high concentration of positively charged residues (blue) in the interhelical region.

interaction between VpU and CD4. The very C-terminal part of CD4 (414–433) is largely unstructured.

Acknowledgment

This work has been supported by a grant from the "Präsidentenfond der Helmholtzgemeinschaft" (HGF, "Virtual Institute of Structural Biology") to D.W.

References

[1] D.S. Wishart, D.A. Case, Methods Enzymol. 338 (2001) 3–34.
[2] S.C. Howell, M.F. Mesleh, S.J. Opella, Biochemistry 44 (2005) 5196–5206.
[3] D.H. Jones, S.J. Opella, J. Magn. Reson. 171 (2004) 258–269.
[4] T. Cierpicki, J.H. Bushweller, J. Am. Chem. Soc. 126 (2004) 16259–16266.
[5] J.J. Chou, J.D. Kaufman, S.J. Stahl, P.T. Wingfield, A. Bax, J. Am. Chem. Soc. 124 (2002) 2450–2451.
[6] M.F. Mesleh, S. Lee, G. Veglia, D.S. Thiriot, F.M. Marassi, S.J. Opella, J. Am. Chem. Soc. 125 (2003) 8928–8935.
[7] L.E. Kay, D.A. Torchia, A. Bax, Biochemistry 28 (1989) 8972–8979.
[8] J. Chung, D. Eliezer, P.E. Wright, H.J. Dyson, Biochemistry 40 (2001) 3561–3571.
[9] T. Stangler, R. Hartmann, D. Willbold, B.W. Koenig, Z. Phys. Chem. 220 (2007) 567–613.
[10] E.R. Zuiderweg, Biochemistry 41 (2002) 1–7.
[11] S.J. Opella, C. Ma, F.M. Marassi, Methods Enzymol. 339 (2001) 285–313.
[12] C.R. Sanders, Hoffmann, A. Kuhn, D.N. Gray, M.H. Keyes, C.D. Ellis, ChemBioChem 5 (2004) 423–426.
[13] U.H. Durr, L. Waskell, A. Ramamoorthy, Biochim. Biophys. Acta 1768 (2007) 3235–3259.
[14] C.R. Sanders, K. Oxenoid, Biochim. Biophys. Acta 1508 (2000) 129–145.
[15] R.D. Krueger-Koplin, P.L. Sorgen, S.T. Krueger-Koplin, I.O. Rivera-Torres, S.M. Cahill, D.B. Hicks, L. Grinius, T.A. Krulwich, M.E. Girvin, J. Biomol. NMR 28 (2004) 43–57.
[16] C. Ma, F.M. Marassi, D.H. Jones, S.K. Straus, S. Bour, K. Strebel, U. Schubert, M. Oblatt-Montal, M. Montal, S.J. Opella, Protein Sci. 11 (2002) 546–557.
[17] K. Oxenoid, H.J. Kim, J. Jacob, F.D. Sonnichsen, C.R. Sanders, J. Am. Chem. Soc. 126 (2004) 5048–5049.
[18] C. Fernandez, K. Adeishvili, K. Wuthrich, Proc. Natl. Acad. Sci. U. S. A. 98 (2001) 2358–2363.
[19] P.J. Maddon, S.M. Molineaux, D.E. Maddon, K.A. Zimmerman, M. Godfrey, F.W. Alt, L. Chess, R. Axel, Proc. Natl. Acad. Sci. U. S. A. 84 (1987) 9155–9159.
[20] W.E. Biddison, P.E. Rao, M.A. Talle, G. Goldstein, S. Shaw, J. Exp. Med. 159 (1984) 783–797.
[21] S.J. Clark, W.A. Jefferies, A.N. Barclay, J. Gagnon, A.F. Williams, Proc. Natl. Acad. Sci. U. S. A. 84 (1987) 1649–1653.
[22] A.G. Dalgleish, P.C.L. Beverly, P.R. Clapham, D.H. Crawford, M.F. Greaves, R.A. Weiss, Nature 312 (1984) 763–767.
[23] D. Klatzmann, E. Champagne, S. Chamaret, J. Gruest, D. Guetard, T. Hercend, J.C. Gluckman, L. Montagnier, Nature 312 (1984) 767–768.
[24] C. Aiken, J. Konner, N.R. Landau, M.E. Lenburg, D. Trono, Cell 76 (1994) 853–864.
[25] S.J. Anderson, M. Lenburg, N.R. Landau, J.V. Garcia, J. Virol. 68 (1994) 3092–3101.
[26] U. Schubert, K. Strebel, J. Virol. 68 (1994) 2260–2271.
[27] F. Margottin, S.P. Bour, H. Durand, L. Selig, S. Benichou, V. Richard, D. Thomas, K. Strebel, R. Benarous, Mol. Cell 1 (1998) 565–574.
[28] M.Y. Chen, F. Maldarelli, M.K. Karczewski, R.L. Willey, K. Strebel, J. Virol. 67 (1993) 3877–3884.
[29] S. Salghetti, R. Mariani, J. Skowronski, Proc. Natl. Acad. Sci. U. S. A. 92 (1995) 349–353.
[30] A. Preusser, L. Briese, A.S. Baur, D. Willbold, J. Virol. 75 (2001) 3960–3964.
[31] M. Wittlich, K. Wiesehan, B.W. Koenig, D. Willbold, Protein Expr. Purif. 55 (2007) 198–207.
[32] M. Wittlich, B.W. Koenig, S. Hoffmann, D. Willbold, Biochim. Biophys. Acta 1768 (2007) 2949–2960.
[33] K. Pervushin, R. Riek, G. Wider, K. Wuthrich, Proc. Natl. Acad. Sci. U. S. A. 94 (1997) 12366–12371.
[34] G. Bodenhausen, D.J. Ruben, Chem. Phys. Lett. 69 (1980) 185.
[35] L.E. Kay, P. Keifer, T. Saarinen, J. Am. Chem. Soc. 114 (1992) 10663–10665.
[36] O. Zhang, L.E. Kay, J.P. Olivier, J.D. Forman-Kay, J. Biomol. NMR 4 (1994) 845–858.
[37] E.R. Zuiderweg, S.W. Fesik, Biochemistry 28 (1989) 2387–2391.
[38] F. Delaglio, S. Grzesiek, G.W. Vuister, G. Zhu, J. Pfeifer, A. Bax, J. Biomol. NMR 6 (1995) 277–293.
[39] R. Keller, The Computer Aided Resonance Assignment Tutorial, CANTINA, Goldau, Switzerland, 2004.
[40] T. Herrmann, P. Guntert, K. Wuthrich, J. Biomol. NMR 24 (2002) 171–189.
[41] T. Herrmann, P. Guntert, K. Wuthrich, J. Mol. Biol. 319 (2002) 209–227.
[42] P. Guntert, K. Wuthrich, J. Biomol. NMR 1 (1991) 447–456.
[43] R. Koradi, M. Billeter, K. Wuthrich, J. Mol. Graph. 14 (1996) 51–55 29-32.
[44] G. Zhu, Y. Xia, L.K. Nicholson, K.H. Sze, J. Magn. Reson. 143 (2000) 423–426.
[45] P. Damberg, J. Jarvet, A. Graslund, Methods Enzymol. 339 (2001) 271–285.
[46] G. Cornilescu, F. Delaglio, A. Bax, J. Biomol. NMR 13 (1999) 289–302.
[47] S.K. Kandasamy, D.K. Lee, R.P. Nanga, J. Xu, J.S. Santos, R.G. Larson, A. Ramamoorthy, Biochim. Biophys. Acta 1788 (2009) 686–695.
[48] D. Willbold, P. Rosch, J. Biomed. Sci. 3 (1996) 435–441.
[49] P.W. Kim, Z.Y. Sun, S.C. Blacklow, G. Wagner, M.J. Eck, Science 301 (2003) 1725–1728.
[50] V. Wray, D. Mertins, M. Kiess, P. Henklein, W. Trowitzsch-Kienast, U. Schubert, Biochemistry 37 (1998) 8527–8538.
[51] J. Yao, J. Chung, D. Eliezer, P.E. Wright, H.J. Dyson, Biochemistry 40 (2001) 3561–3571.
[52] U.H. Durr, K. Yamamoto, S.C. Im, L. Waskell, A. Ramamoorthy, J. Am. Chem. Soc. 129 (2007) 6670–6671.
[53] V. Wray, T. Federau, P. Henklein, S. Klabunde, O. Kunert, D. Schomburg, U. Schubert, Int. J. Pept. Protein Res. 45 (1995) 35–43.
[54] D. Willbold, S. Hoffmann, P. Rösch, Eur. J. Biochem. 245 (1997) 581–588.